ANNALS OF GEOPHYSICS, 69, 5, T556, 2026; doi:10.4401/ag-9593
OPEN ACCESS

Global Persistence of Intraplate Heat-Flow Anomalies Reveals Limits of Tectonic Distance Control

Cristiano Gaujac*,1

(1) Independent Researcher, Villefranche-sur-Saône, France

Article history: received April 26, 2026; accepted September 9, 2026

Abstract

Surface heat flow is usually interpreted in plate-tectonic terms: high values are expected near active boundaries, whereas lower values are expected in more stable intraplate regions. What is still uncertain, however, is how much of the global variability observed within the intraplate domain can really be explained by tectonic proximity alone.

To address that question, we carried out a global point-by-point analysis of the 2024 release of the IHFC Global Heat Flow Database, combined with two independent tectonic datasets: the GEM Global Active Faults Database and the PB2002 plate-boundary model. Within a fully reproducible workflow, we defined a canonical intraplate domain as all observations located at least 110 km from the nearest mapped tectonic structure (dist_min_km ≥ 110 km; N = 53,420).

Within this canonical dataset, heat flow decreases on average with tectonic distance, but the effect is weak. In log-log space, the main regression yields a negative slope (β about −0.11) and low explanatory power (R^2 about 0.06-0.10). At the same time, high heat-flow values remain present across the full range of tectonic distances, including regions located more than 2,000 km from mapped tectonic structures.

We then applied three independent geophysical screening tests based on shallow seismicity, lithospheric strain rate, and Bouguer gravity anomalies. After this screening, 603 intraplate thermal anomalies remain.

Taken together, these results show that tectonic distance captures part of the broad background structure of the global thermal field, but it does not explain the full variability of intraplate heat flow. The persistence of a geographically dispersed residual component therefore provides a quantitative observational constraint that is not represented by first-order tectonic models and should be considered in future geodynamic interpretations of Earth's thermal field.

Keywords: Heat Flow; Intraplate; Tectonic Distance; Lithosphere; Thermal Anomalies

1. Introduction

Earth's thermal evolution influences plate dynamics, mantle convection, and the transfer of heat from the interior to the surface. Surface heat flow is one of the clearest observational windows into these processes because it integrates the effects of lithospheric structure, radiogenic heat production, and deeper mantle dynamics (Jaupart et al., 2015).

Global estimates suggest that Earth loses roughly 40-45 TW of heat, with first-order variations related to lithospheric age, thermal structure, and tectonic regime (Pollack et al., 1993; Davies and Davies, 2010). Even so, the global heat-flow field remains difficult to interpret in a simple way, partly because the database itself is spatially uneven and affected by known sampling biases (Davies, 2013; Lucazeau, 2019; Stål et al., 2022).

At broad scales, plate tectonics provides a natural starting point for interpreting heat-flow variability. Classical models predict higher values near plate boundaries and lower values in mature intraplate regions, mainly because lithosphere cools and thickens away from active tectonic margins (Sclater and Francheteau, 1970; Stein and Stein, 1992). This framework is useful, but it does not fully answer a basic empirical question: how much of the observed variability in intraplate heat flow is actually controlled by tectonic distance?

This question matters because global compilations show that elevated heat-flow values are not confined to plate boundaries. They also occur in regions far from active tectonic structures (Goutorbe et al., 2011; Lucazeau, 2019). Those elevated values may reflect lithospheric heterogeneity, deeper mantle processes, or other controls that are not captured by tectonic proximity alone. However, the relative importance of tectonic distance has not been tested systematically at the global scale using a point-by-point framework.

Another limitation of earlier work is that the intraplate domain is often treated implicitly instead of being defined through a reproducible observational protocol. Regional studies, pre-aggregated data, and qualitative tectonic classifications can all obscure the structure of the global signal. A clearer test therefore requires both a reproducible definition of what counts as intraplate and a consistent way to evaluate heat flow across the full range of tectonic distances.

In this study, we address both issues through a fully reproducible global workflow built on the IHFC heat-flow database and two independent tectonic datasets. We first define a canonical intraplate domain from empirical distance diagnostics. We then test whether tectonic proximity provides a sufficient explanation for intraplate heat-flow variability, or whether a robust residual population of anomalies persists at large distances from mapped tectonic structures.

Our goal is not to assign a single physical mechanism to that residual variability. Rather, it is to establish a clear observational constraint: if high intraplate heat-flow values remain widespread even after conservative tectono-geophysical screening, then proximity to mapped tectonic structures cannot by itself explain the global intraplate thermal field.

2. Data and Methods

Heat-flow data were taken from the 2024 release of the IHFC Global Heat Flow Database, whose updated structure and quality-control framework are described by Fuchs et al. (2023). The raw catalog contains 91,182 entries. We first applied a fully programmatic validation step so that only physically meaningful observations entered the analysis. This step included numeric type coercion, removal of missing or non-numeric values, and exclusion of non-physical measurements ($q \leq 0$). After validation, 91,059 physically valid observations remained. No interpolation, smoothing, or model-based correction was applied, so the analysis reflects the observed database as directly as possible.

We measured tectonic proximity by asking a simple geographic question for every heat-flow observation: how far is the site from the nearest mapped active fault or plate boundary? To answer it independently of any single tectonic map, we combined the GEM Global Active Faults Database (Styron and Pagani, 2020) with the PB2002 plate-boundary model (Bird, 2003). Both datasets were first harmonized in the WGS84 geographic coordinate system (EPSG:4326), so that all locations shared the same latitude-longitude reference. Their geometries were then cleaned and standardized, and spatial indices were built for efficient global point-to-line calculations.

For each observation, we calculated the distance to the nearest structure in each tectonic dataset and retained the smaller of the two values: dist_min_km = min (dist_gem_km, dist_pb_km). Thus, a site was considered tectonically close whenever either dataset mapped a structure nearby. Because latitude and longitude are angular coordinates rather than direct distance units, the geometries were temporarily converted to a metric coordinate system (EPSG:3857) for the distance calculations. Independent checks using local azimuthal equidistant projections, which preserve distances more accurately around each observation, confirmed that projection-related distortion did not change the intraplate classification at the adopted scale.

We defined the intraplate domain from the behavior of the observations rather than from a conventional fixed distance. The validated catalog was divided into distance classes (0-50, 50-100, 100-150, 150-300, and

300-1,000 km), and we tracked how median heat flow and its 90th percentile changed among them (Fig. 1). The statistics identify a transition from stronger boundary influence to a comparatively stable regime. We therefore adopted dist_min_km ≥ 110 km as a conservative operational definition of the intraplate domain.

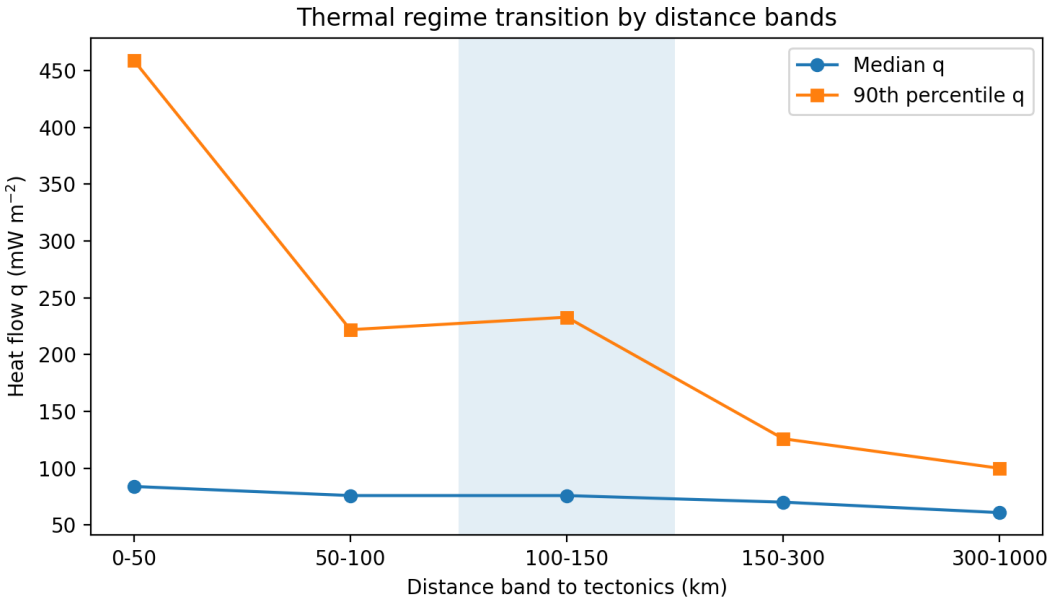

Figure 1. Change in heat-flow distributions across tectonic-distance bands. Median and 90th-percentile surface heat flow (q) calculated within five bands of minimum distance to mapped tectonic structures (0-50, 50-100, 100-150, 150-300, and 300-1,000 km). The shaded category marks the 100-150 km band, interpreted as an approximate transition between observations more strongly influenced by nearby tectonic structures and the more distant intraplate domain. This binned diagnostic motivates the location of the operational cutoff but does not identify 110 km as a unique statistical breakpoint.

Based on this approximate transition, we selected 110 km as a conservative operational cutoff within the 100-150 km band. We also repeated the analysis using alternative cutoffs from approximately 80 to 150 km. Median and 90th-percentile heat flow varied only modestly across these alternatives, and the main conclusions remained unchanged. Thus, 110 km is an operational choice within a robust interval rather than a unique statistical breakpoint. The complete threshold-sensitivity diagnostic is provided in Supplementary Fig. SM2.

Heat-flow values have a strongly asymmetric distribution, with a long upper tail. We therefore analyzed both heat flow and tectonic distance on logarithmic scales, which reduces skewness and allows proportional changes to be compared more directly. The relationship tested throughout the paper is $\log_{10}(q)$ versus $\log_{10}(\text{dist_min_km} + 1)$; adding 1 avoids taking the logarithm of zero without materially affecting larger distances.

We estimated this relationship in the main point-by-point intraplate dataset using ordinary least-squares (OLS) regression with HC3 robust standard errors. In plain terms, HC3 errors make the uncertainty estimates less sensitive to unequal scatter across the data. We then repeated the analysis after combining nearby measurements into sites at scales of approximately 0.5-2 km, using weighted and unweighted variants. These supporting tests ask whether dense local sampling or repeated nearby measurements could create the observed global relationship; they do not replace the main point-by-point analysis.

The canonical intraplate dataset was defined directly at point level by applying the cutoff dist_min_km ≥ 110 km to the validated catalog. No spatial aggregation was used at this stage. To ensure reproducibility, the dataset was generated deterministically and associated with a cryptographic fingerprint.

To identify intraplate thermal anomalies, we applied a conservative physical threshold of $q \geq 169\ \text{mW m}^{-2}$. This value was derived from reproducible diagnostics of the upper tail of the global heat-flow distribution and was used only to define the subset of candidate anomalies for further screening.

Candidate anomalies were then passed through a multi-source quality-control procedure applied strictly at point level, without spatial aggregation. This screening consisted of three independent rejection tests: A for

shallow seismicity, B for strain rate, and C for Bouguer gravity. Observations were retained only when none of these indicators was triggered.

In Test A, candidate points were rejected if they were within 50 km of a shallow earthquake or if the annual rate of shallow seismicity within 100 km exceeded 2 events per year.

In Test B, candidate points were rejected if the local strain-rate value from GSRM v2.1 (Kreemer et al., 2014) exceeded 1×10^{-9}.

In Test C, candidate points were rejected if their local Bouguer gravity value from the World Gravity Map (Bonvalot et al., 2012) differed strongly from a surrounding 300-500 km reference annulus, based on a robust z-score threshold of $|z| \geq 2.0$.

These three filters were applied independently. The final retained intraplate subset therefore consists of points that satisfy the geometric intraplate definition, exceed the thermal threshold, and are not removed by these operational tectono-geophysical controls.

All analyses were performed within a deterministic and fully reproducible pipeline, with explicit separation between exploratory and canonical artifacts, protocol logging, and integrity verification of frozen outputs.

To test context beyond distance, canonical intraplate observations were assigned to the nearest typed plate-boundary environment using the UTIG layer hosted by NOAA/NCEI (NOAA NCEI, n.d.). Continental models then added Moho depth from the $1° \times 1°$ CRUST1.0 grid (Laske et al., 2013), whereas oceanic models added seafloor age from the global age grid of Müller et al. (2008). Each context variable was evaluated as an addition to the distance-only regression, so the change in explained variance measures incremental contextual information rather than direct physical source partitioning.

The present framework is observational and does not directly partition surface heat flow into crustal radiogenic and mantle-derived convective components. Instead, where additional physical context is evaluated, it is introduced through simple proxies tied to crustal structure and lithospheric thermal evolution. These proxies are used to test whether tectonic distance alone is sufficient, not to claim a direct source decomposition of the heat-flow signal. This distinction follows established treatments of lithospheric heat production and thermal structure (Furlong and Chapman, 2013; Hasterok and Chapman, 2011; Jaupart et al., 2015).

Further technical details on geometric audits, distance-model consistency, and the exact implementation of the screening tests are given in the Supplementary Methods.

3. Results

Applying the intraplate criterion (dist_min_km ≥ 110 km) yields 53,420 observations, which define the main analytical dataset (Fig. 2). We first asked whether heat flow changes systematically with tectonic distance. In log-log space, heat flow decreases on average as distance increases (Fig. 3a), but the effect is modest: the slope is about −0.11, and tectonic distance explains only about 6-10% of the point-by-point variability. A tenfold increase in (dist_min_km + 1) corresponds to an average heat-flow reduction of about 23%. The association is statistically clear ($p < 10^{-15}$), yet the wide scatter shows that distance alone is a weak predictor of heat flow at any particular site.

The distance-class analysis (Fig. 3b) makes the same pattern easier to see. Median heat flow declines progressively with increasing tectonic distance, but elevated values remain present in every class, including those beyond 2000 km. The spread of the distributions and the relative frequency of extreme values both decline with distance, but they do not disappear. This persistence matters because it shows that tectonic isolation does not produce a uniformly cool or uniform intraplate domain. Instead, thermally elevated observations remain part of the empirical structure of the dataset even where distance from mapped tectonic structures is large.

We next tested whether this gradient could be caused by dense or uneven spatial sampling. After nearby measurements were combined into sites at scales of 0.5-2 km, the slope remained negative and changed by less than 0.03 relative to the main point-by-point fit (Fig. 4a). The site-level regression gives a slope of about −0.113 (95% confidence interval, approximately −0.116 to −0.109) and R^2 of about 0.096; weighted analyses give similar values. Thus, spatial aggregation changes neither the direction nor the approximate magnitude of the relationship. The low R^2 reflects limited explanatory power, whereas the stability across sampling treatments shows that the underlying gradient is robust.

We then asked whether a particular continent or a small number of extreme observations drives the result. It does not: when each continent is omitted in turn, or when the most extreme 0.5% at both ends of the distribution are

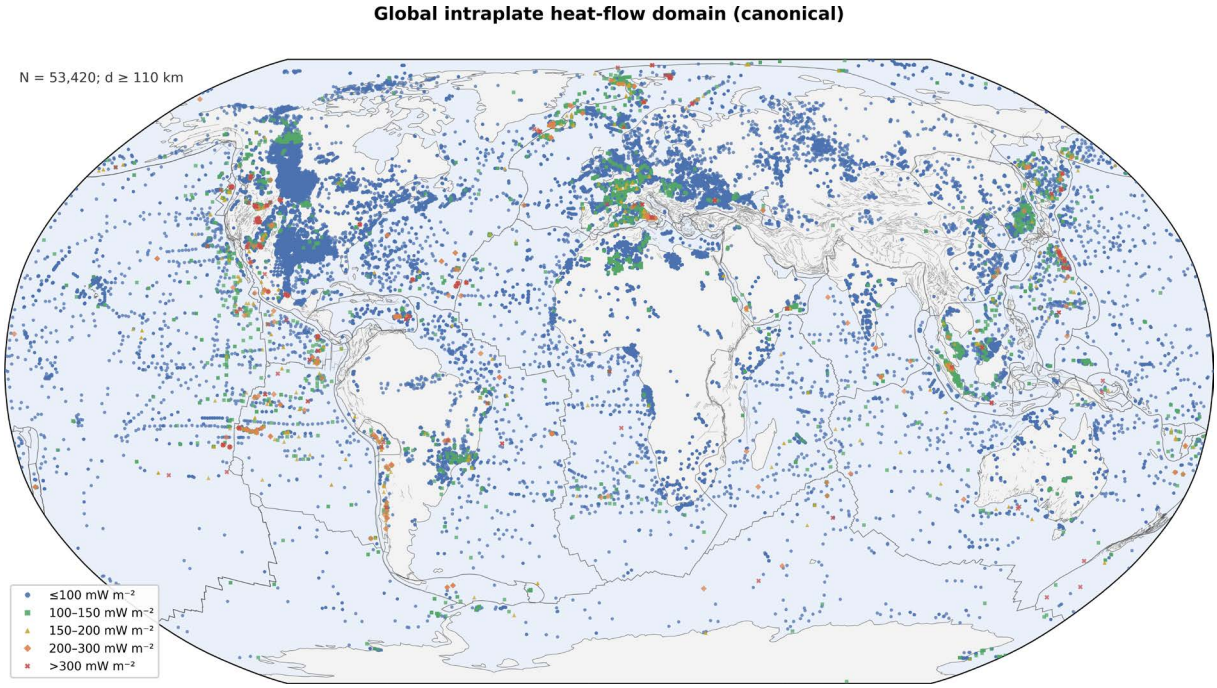

Figure 2. Canonical intraplate heat-flow domain. Global distribution of the canonical intraplate heat-flow dataset (N = 53,420), defined by a minimum distance of 110 km from the nearest mapped tectonic structure. Each point represents an individual heat-flow measurement projected in a Robinson coordinate system. Colors indicate measured heat-flow values (q, mW m^{-2}). Major mapped fault systems from the GEM Global Active Faults Database and the PB2002 plate-boundary model are shown as contextual overlays. This figure defines the observational domain used for all subsequent analyses.

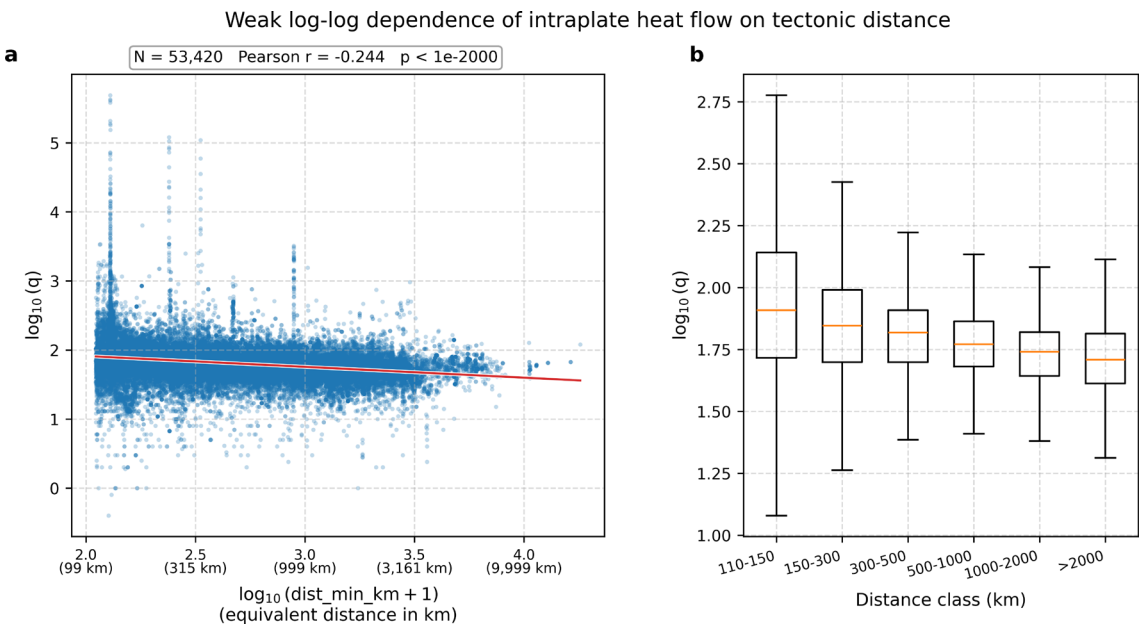

Figure 3. Weak log-log dependence of intraplate heat flow on tectonic distance. (a) Scatterplot of $\log_{10}(q)$ versus $\log_{10}(\text{dist_min_km} + 1)$ for all intraplate measurements (dist_min_km ≥ 110 km). Each point represents an individual IHFC site. The red line indicates the ordinary least-squares linear regression in log-log space. A weak negative trend is observed, accompanied by large dispersion across the full distance range. (b) Boxplots of $\log_{10}(q)$ stratified by distance classes (110-150, 150-300, 300-500, 500-1000, 1000-2000, >2000 km). Median heat flow decreases progressively with increasing distance, yet elevated values persist in all classes, indicating substantial intraplate heterogeneity that cannot be explained by tectonic distance alone.

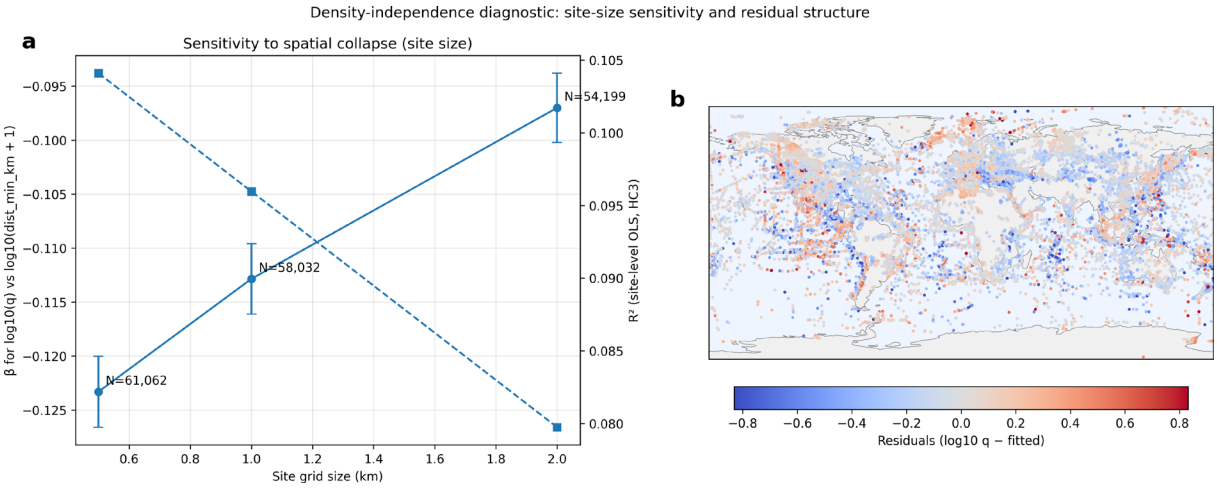

Figure 4. Sampling-density diagnostic: site-size sensitivity and residual structure. (a) Sensitivity of the regression slope β of $\log_{10}(q)$ versus $\log_{10}(\text{dist_min_km} + 1)$ to the spatial collapse cell size used to define analytical sites (0.5, 1, and 2 km). Points show estimated β values (OLS with HC3 robust errors), with bars indicating 95% confidence intervals. The dashed line indicates variation in the coefficient of determination (R^2) at each scale. N values denote the number of valid sites used. (b) Global map of site-level residuals from the fitted model (observed – fitted $\log_{10}(q)$). Colors indicate residual magnitude and sign. No systematic tectonic alignment or coherent global spatial organization is observed.

removed, the sign and approximate magnitude of the association remain stable, and the slope changes by less than about ±0.02 (Fig. 5).

The mean relationship also does not describe all parts of the heat-flow distribution equally well. Quantile regression shows a stronger distance effect among unusually high values than among typical values, with the slope approaching −0.32 at the 90th percentile and the contrast being greatest in the oceanic domain (Fig. 6). In practical terms, tectonic distance is more closely related to the upper heat-flow extremes than to the center of the distribution.

Having established that the global gradient is robust, we next asked whether it varies among different tectonic settings. The slope remains negative when observations are stratified by their nearest convergent, divergent, or transform boundary context in the UTIG plate-boundary layer hosted by NOAA/NCEI (NOAA NCEI, 2026), but its strength differs markedly (Fig. 7). It is weakest in the convergent context (slope about −0.093; R^2 about 0.022), intermediate in the divergent context (about −0.164; R^2 about 0.061), and strongest in the transform context (about −0.252; R^2 about 0.184). These differences indicate that the expression of the tectonic-distance gradient varies among structural settings rather than following a uniform global relationship.

We then tested which broad geological variables might add explanatory context beyond tectonic distance. In continental regions, adding Moho depth from CRUST1.0 (Laske et al., 2013) raises R^2 from about 0.034 to 0.058. In oceanic regions, adding seafloor age from Müller et al. (2008) raises R^2 from about 0.109 to 0.199 (Fig. 8), while median heat flow decreases from about 105 mW m^{-2} in young crust to about 50 mW m^{-2} in old crust. No single variable replaces tectonic distance. Instead, the results support a layered explanation: boundary setting modifies the distance relationship, while crustal structure and lithospheric age explain additional domain-specific variability. These proxies improve interpretation but do not identify a unique heat source.

Finally, we asked whether the highest intraplate values persist after independent screening for more immediate geophysical explanations. The threshold $q \geq 169$ mW m^{-2} identifies 1,764 candidates. Filters based on shallow seismicity, deformation rate, and gravity retain 603 observations, or about 34.2% of the candidates. These points do not prove a common mechanism, but their persistence shows that many elevated intraplate measurements cannot be removed by the first-order controls tested here.

The retained subset remains globally distributed (Fig. 9). All observations lie beyond the 110 km intraplate cutoff. Approximately 49% are located more than 300 km from mapped tectonic structures, 34% more than 500 km away, and about 13% more than 1000 km away. The median tectonic distance of the retained subset is about 289 km, and maximum values exceed 4000 km.

a

Perturbation	R	β	N
Full global dataset	-0.244	-0.157	53,420
Excluding Africa	-0.250	-0.162	49,282
Excluding Antarctica	-0.246	-0.158	53,368
Excluding Asia	-0.241	-0.155	51,103
Excluding Europe	-0.212	-0.142	44,362
Excluding North America	-0.255	-0.174	38,686
Excluding Oceania	-0.244	-0.157	52,838
Excluding South America	-0.248	-0.160	52,396
Excluding Unknown	-0.268	-0.135	31,905
Trimmed 0.5–99.5%	-0.264	-0.140	52,884

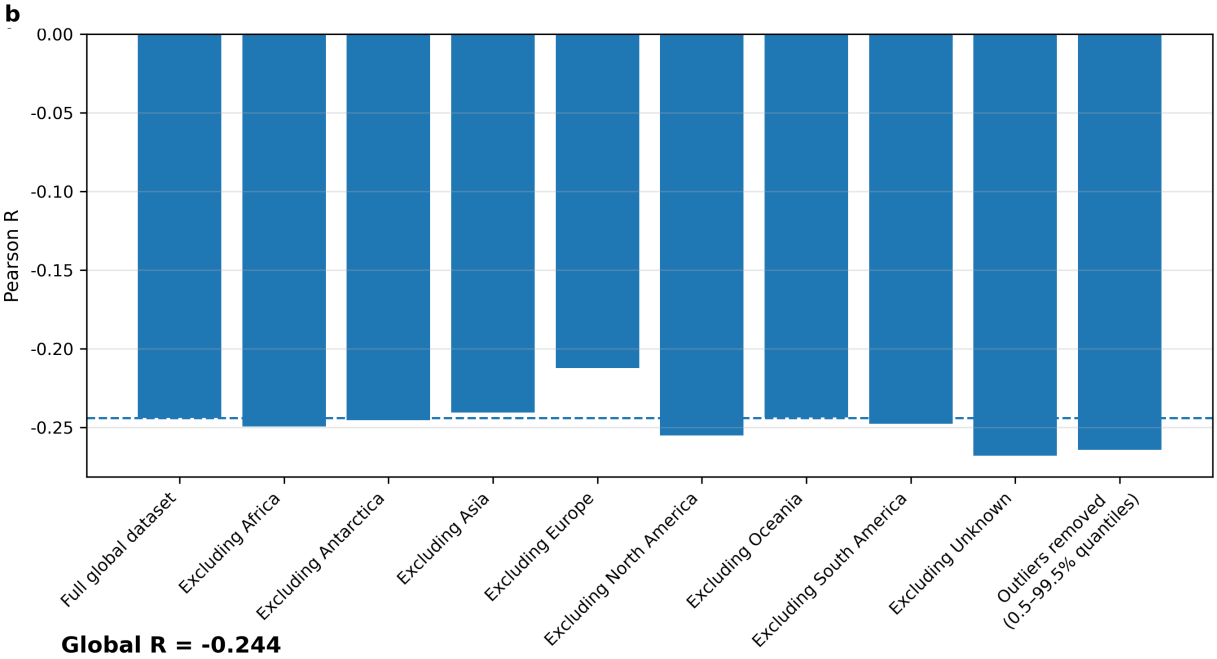

Figure 5. Robustness of the global intraplate gradient to regional exclusion and tail trimming. (a) Robustness summary of the Pearson correlation coefficient (r), regression slope (β), and sample size (N) for $\log_{10}(q)$ versus $\log_{10}(\text{dist_min_km} + 1)$ in the canonical intraplate domain ($\text{dist_min_km} \geq 110$ km), calculated for the full dataset, leave-one-continent-out subsets, and a symmetrically trimmed dataset (0.5-99.5%). (b) Corresponding Pearson r values for each perturbation, with the dashed line indicating the full-dataset value. The overall similarity of the coefficients across perturbations shows that the observed negative gradient is not driven by any single continental domain or by a small number of extreme values.

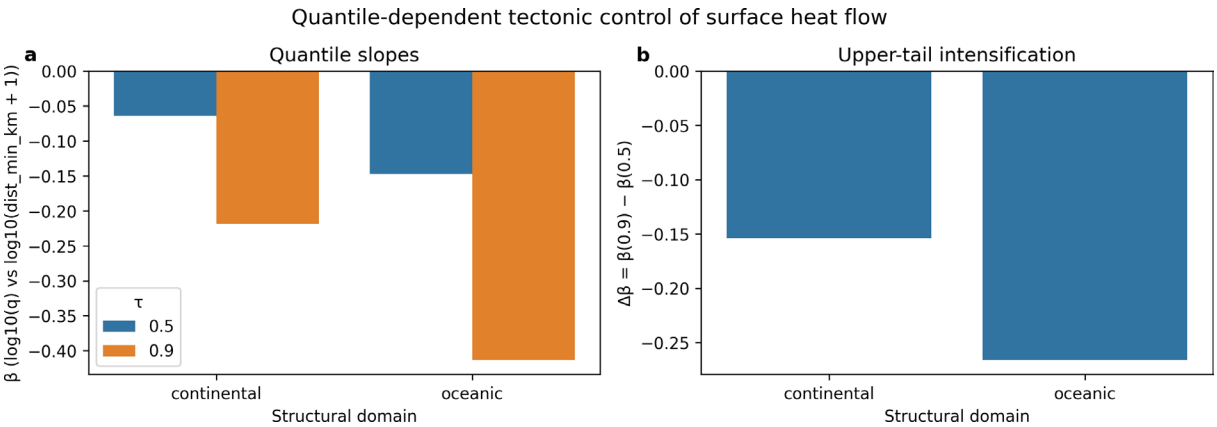

Figure 6. Quantile-dependent tectonic control of surface heat flow. (a) Quantile-regression slope coefficients (β) for the relationship between $\log_{10}(q)$ and $\log_{10}(\text{dist_min_km} + 1)$ at $\tau = 0.5$ and $\tau = 0.9$, estimated separately for continental and oceanic domains. (b) Upper-tail intensification, expressed as $\Delta\beta = \beta(0.9) - \beta(0.5)$, showing that the negative association between heat flow and tectonic distance strengthens toward the upper tail of the distribution. The larger values of $|\beta|$ and $\Delta\beta$ in the oceanic domain indicate that high heat-flow extremes there are more sensitive to tectonic distance than in the continental domain.

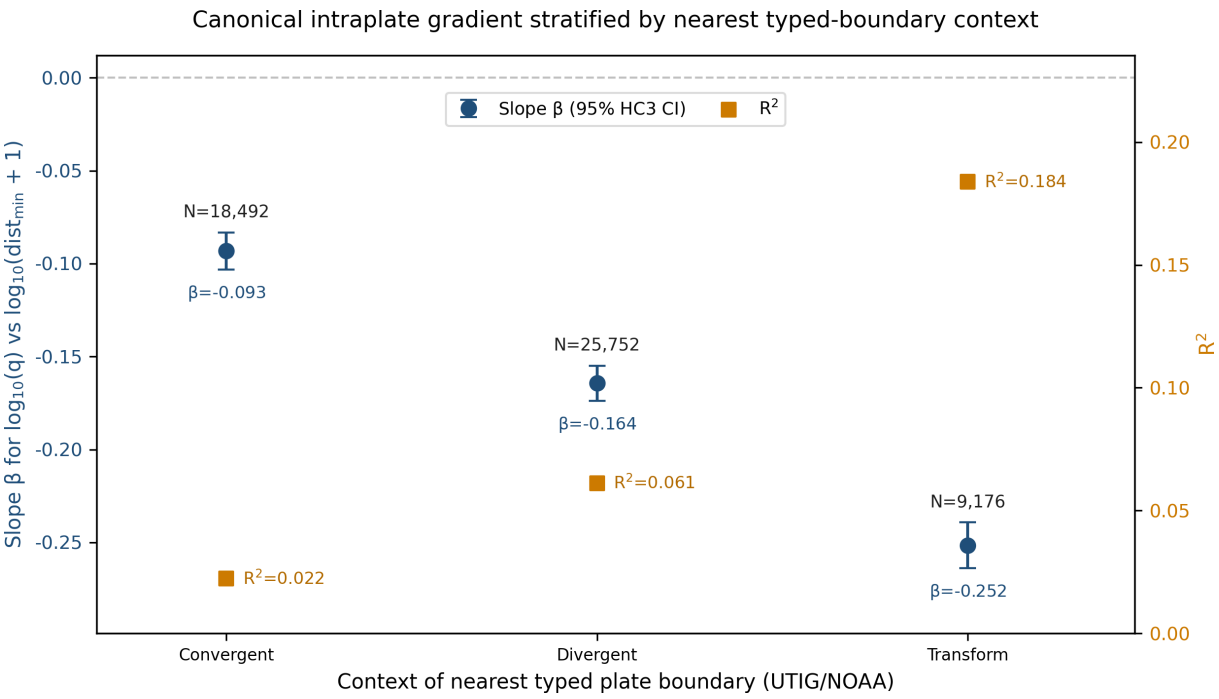

Figure 7. Canonical intraplate gradient stratified by nearest typed-boundary context. Blue points show the OLS slopes (β) for $\log_{10}(q)$ versus $\log_{10}(\text{dist_min_km} + 1)$, with 95% confidence intervals based on HC3 robust standard errors. Orange squares show the corresponding coefficients of determination (R^2). Canonical intraplate observations are stratified by the nearest convergent, divergent, or transform boundary context identified from a densified representation of the UTIG/NOAA typed plate-boundary layer, while the regression retains the canonical tectonic-distance metric, dist_min_km. The gradient remains negative in all three contexts but is weakest for convergent, intermediate for divergent, and strongest for transform settings.

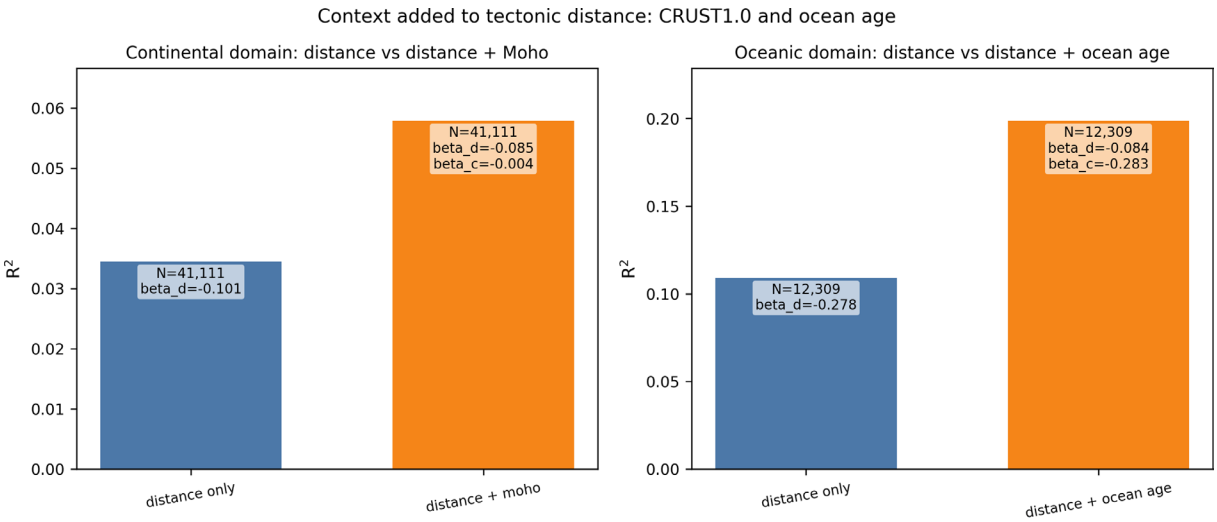

Figure 8. Context added to tectonic distance: CRUST1.0 and ocean age. Comparison between distance-only models and models that add simple lithospheric-context proxies to the canonical intraplate regressions: Moho depth from CRUST1.0 in the continental domain and seafloor age in the oceanic domain. Bars show explained variance (R^2), and in-panel labels report sample size and regression coefficients. The gain in explanatory power is modest in the continental domain and stronger in the oceanic domain, indicating that domain-specific lithospheric context improves interpretation relative to tectonic distance alone.

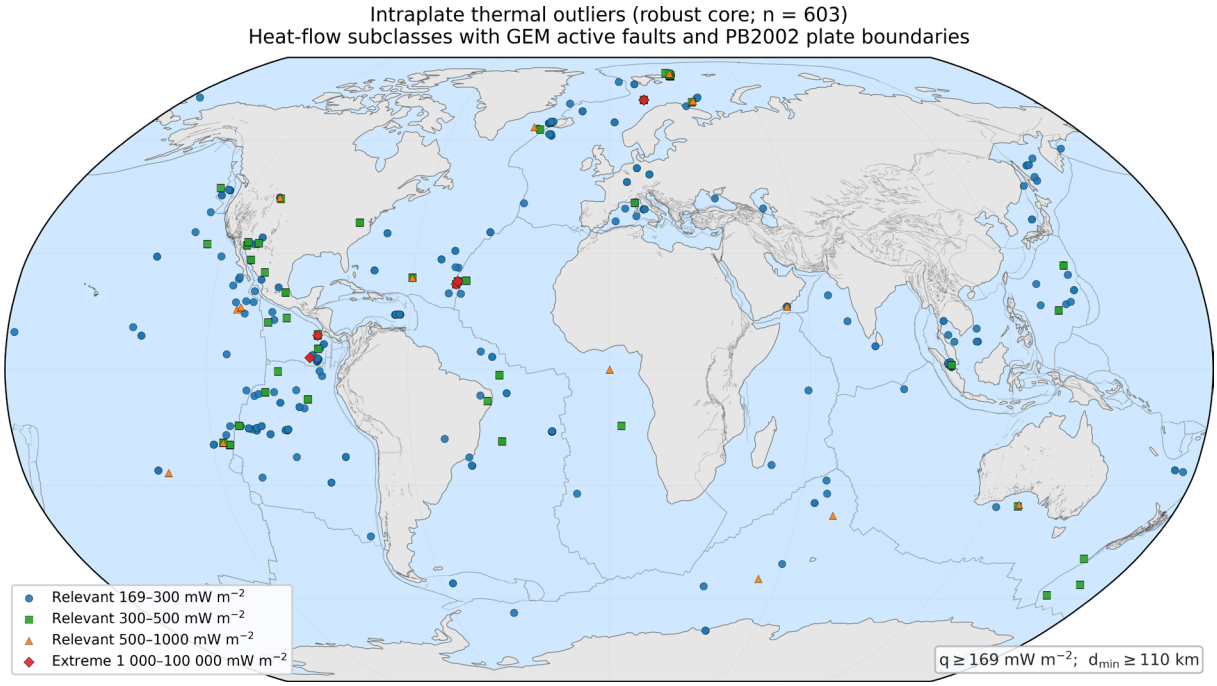

Figure 9. Global distribution of robust intraplate thermal anomalies. Global map of the 603 intraplate measurements retained after all tectono-geophysical screening steps. Symbols indicate heat-flow subclasses (169-300, 300-500, 500-1000, and >1000 mW m^{-2}). All sites lie at least 110 km from any mapped active fault (GEM) or plate boundary (PB2002). Their dispersed spatial distribution, without persistent linear alignments or simple tectonic patterns, indicates that these anomalies are not systematically organized by plate-boundary geometry and are not readily attributable to the first-order tectono-geophysical controls evaluated here.

Residuals, defined as observed minus fitted values of $\log_{10}(q)$, are centered near zero but retain long tails and show no persistent linear alignment or dominant global spatial pattern (Fig. 4b). The Results therefore establish three linked findings: a weak but robust negative distance gradient, substantial variability at every distance, and a geographically dispersed population of elevated values that survives conservative screening.

4. Discussion

The central result is straightforward: heat flow decreases on average with distance from mapped tectonic structures, but distance explains only a small fraction of the global intraplate variability (Davies and Davies, 2010; Goutorbe et al., 2011; Lucazeau, 2019). The low R^2 does not make the gradient meaningless; it shows that proximity captures a broad background component rather than predicting individual sites. Elevated values remain even 1,000-2,000 km from mapped structures, confirming that the intraplate domain is thermally heterogeneous. This pattern agrees with global compilations (Pollack et al., 1993; Davies, 2013; Lucazeau, 2019; Stål et al., 2022) and persists after independent screening for shallow tectono-geophysical contexts.

The comparison between continental and oceanic domains helps clarify this point. The negative relation between heat flow and tectonic distance appears in both settings, so it is not restricted to one type of lithosphere. However, the relation is expressed differently in each domain. The oceanic dataset shows broader thermal dispersion and a stronger upper tail, suggesting that the average distance signal is superimposed on different thermal background states linked to lithospheric age, conductive cooling, and hydrothermal or mantle-related processes (Sclater et al., 1980; Stein and Stein, 1992). In other words, the main trend is global, but its meaning is not exactly the same everywhere. This is why the distinction between continental and oceanic behavior matters for interpretation (Fig. 10).

The boundary-type analysis refines the same point from a different angle. The negative gradient persists whether the nearest typed plate-boundary context is convergent, divergent, or transform, but its strength differs markedly among those settings. This means that tectonic proximity does not operate in a uniform way across all structural

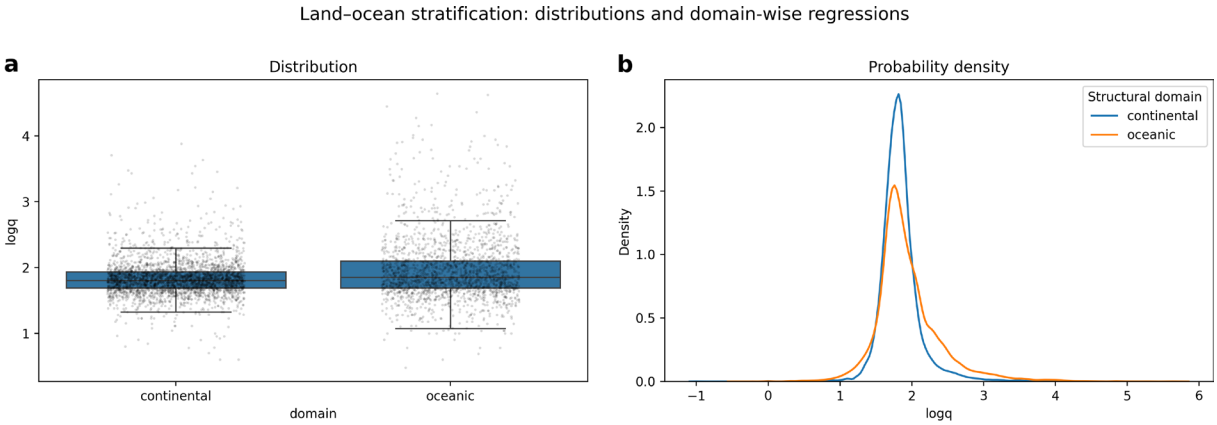

c

beta	se	ci_low	ci_high	R2	N	domain
-0.096489	0.001614	-0.099653	-0.093326	0.08712	54220	continental
-0.189615	0.002948	-0.195393	-0.183838	0.107112	36839	oceanic

Slope-difference z-test: z=27.710, p=0.000e+00

Figure 10. Land-ocean stratification of heat flow: distributions and domain-wise regressions. (a) Distribution of $\log_{10}(q)$ for continental and oceanic structural domains, showing greater dispersion and a more pronounced upper tail in the oceanic domain. (b) Kernel density estimates of $\log_{10}(q)$ by domain, showing stronger positive skewness and a shift toward higher values in the oceanic domain. (c) OLS regressions with HC3 robust standard errors for the model $\log_{10}(q) \sim \log_{10}(\text{dist_min_km} + 1)$, fitted separately by structural domain. The oceanic domain shows a significantly more negative slope (β = -0.1896) than the continental domain (β = -0.0965). The difference in slopes is statistically significant ($z = 27.71$, $p < 1 \times 10^{-15}$).

environments. Instead, the observed global relation appears to be modulated by the tectonic character of the nearest boundary context. That result does not identify a mechanism by itself, but it does show that a single global distance law is too simple to describe the full intraplate signal.

Together, the boundary-type, CRUST1.0, and ocean-age analyses provide a concrete answer to what can complement tectonic proximity. Boundary setting changes the strength of the distance gradient; Moho depth adds modest continental context; and seafloor age provides a stronger oceanic constraint linked to lithospheric cooling. The result is not a single replacement variable but a domain-aware framework that combines tectonic distance with physically meaningful information about crustal structure and lithospheric evolution.

This layered framework explains more than a single global distance law, yet it remains incomplete. Even after the added context and independent screening, 603 elevated intraplate observations remain unexplained by the first-order controls evaluated here.

The scope of that conclusion is important. The study does not quantify the fractions of surface heat flow derived from crustal radioactivity and mantle convection, either globally or at individual sites. The available proxies indicate where crustal structure and lithospheric history improve interpretation, but they cannot assign each residual anomaly to a unique crustal or mantle source.

Several tests support this interpretation. First, the gradient survives spatial aggregation, showing that it is not simply an artifact of dense local sampling or nearby repeated measurements. Aggregation is used only as a robustness test; the main dataset remains point-by-point because that level of observation defines the analytical protocol.

Second, the 110 km cutoff should be understood as an operational boundary rather than a sharp geodynamic divide. It marks the point at which the thermal statistics become more stable, not the point at which Earth processes suddenly change. This is an important distinction. The study does not claim that tectonic and intraplate regimes are separated by a rigid physical threshold. Rather, it defines a conservative and reproducible analytical domain within which the central question can be tested consistently.

Third, the result does not depend strongly on one specific geometric representation of tectonic structure. The comparison between independent tectonic models and the geometric audits both point in the same direction: the observed global pattern is not a fragile artifact of one catalog or one mapping choice. Using the minimum distance

to either GEM or PB2002 helps reduce sensitivity to local mapping gaps or geometry-specific effects (Bird, 2003; Styron and Pagani, 2020). This does not make the distance metric perfect, but it does show that the main signal is not critically dependent on one particular tectonic dataset.

The form of the statistical model also follows the data. Raw heat-flow values are strongly right-skewed, so logarithmic transformation reduces the dominance of the upper tail, and robust errors accommodate unequal scatter. Some residual asymmetry remains, but this is expected in a heterogeneous observational dataset and does not by itself invalidate the central gradient (Lucazeau, 2019; Stål et al., 2022; Fuchs et al., 2023).

Geodynamically, the results favor a layered rather than a single-control interpretation. Tectonic distance describes part of the broad background pattern; lithospheric age and crustal structure add domain-specific information; and a dispersed residual component remains. Classical cooling models are especially informative in the oceanic domain (Fig. 10), but the remaining variability also leaves room for lithospheric heterogeneity, local processes, and deeper mantle contributions that cannot be separated with the present data.

Quantile regression adds one further constraint: the distance effect is stronger among the highest heat-flow values than near the middle of the distribution (Fig. 6). Tectonic proximity therefore shapes part of the upper tail, but still leaves much of the intraplate variability unexplained.

At the same time, the artificial-lineament control places an important limit on interpretation. Because lineaments of comparable density can reproduce correlations of similar magnitude, part of the point-to-line signal may arise from general geometric properties of the problem and from the spatial organization of the sampling itself. This does not invalidate tectonic distance as an observational variable, but it does require restraint. The relationship documented here should remain observational in interpretation and should not be presented as a strong causal demonstration at the global scale.

The 603 screened anomalies illustrate both the importance and the limit of the result. Their persistence and lack of systematic alignment with major tectonic structures (Fig. 9) mean that they cannot be dismissed as a few extreme measurements or as the simple product of one screened proxy. Local processes, including mantle plumes, may explain individual cases (Courtillot et al., 2003), but no single tested mechanism accounts for the globally dispersed population. The subset is therefore evidence of unresolved variability, not proof of a common origin.

The supplementary clustering analyses are compatible with this same picture. They show that intraplate variability has detectable internal structure, but not one that resolves into robust and uniquely stable discrete groups across methods. This argues against a simple partition of the intraplate thermal field into a few sharply separated classes and instead supports a more continuous view in which several controls overlap in feature space.

The observations can thus be organized into two levels: a broad background trend associated with tectonic setting and lithospheric evolution, and a spatially dispersed residual component that remains after this background and the screening tests are considered. The second level identifies what future geodynamic models must explain; it does not, by itself, identify one physical mechanism.

Separating that residual signal into crustal radiogenic and mantle-derived convective contributions will require additional global constraints, particularly spatially resolved information on crustal heat production, lithospheric structure, and mantle thermal variability (Furlong and Chapman, 2013; Hasterok and Chapman, 2011; Jaupart et al., 2015). That source decomposition is therefore a specific next step rather than a claim of the present study.

More broadly, the results show that intraplate variability is not adequately represented as random noise around an average tectonic trend. Its persistence across robustness tests, independent filters, and complementary geological contexts demonstrates the limits of tectonic distance as a stand-alone predictor (Davies, 1980; Pollack et al., 1993; Davies and Davies, 2010). Future models of Earth's thermal field should therefore treat this variability as a feature to be explained, not merely as scatter to be removed (Pollack et al., 1993; Jaupart et al., 2015).

5. Conclusions

This study shows that tectonic distance is negatively related to intraplate heat flow, but with low explanatory power at the global scale. Elevated values persist across the full distance range, including regions that are highly isolated from tectonic structures.

Even after independent geophysical filters are applied, a robust subset of intraplate anomalies remains. This indicates that tectonic proximity is not a sufficient predictor of global thermal variability. The results therefore define a quantitative observational constraint that is not captured by first-order tectonic models and should be incorporated into future geodynamic approaches.

Data availability statement. All primary datasets used in this study are publicly available from their original sources.
The IHFC Global Heat Flow Database (2024 release) is available at https://doi.org/10.5880/fidgeo.2024.014.
The GEM Global Active Faults Database is available at https://github.com/GEMScienceTools/gem-global-active-faults.
The PB2002 plate-boundary model is available at https://doi.org/10.1029/2001GC000252.
The global earthquake catalog is available from the U.S. Geological Survey at https://earthquake.usgs.gov/earthquakes/search/.
Additional datasets, including the Global Strain Rate Model (GSRM v2.1) and the World Gravity Map (WGM2012), are available from their respective published sources.
Curated contextual inputs used for the typed-boundary, crustal-thickness, and ocean-age analyses are distributed with the GitHub repository under data/raw/, with their provenance and original sources documented therein.
The complete reproducible analysis pipeline is publicly available at: https://github.com/gaujac/heatflow-intraplate-residuals
A frozen reproducibility archive containing all figures, derived datasets, and pipeline outputs used in this study is available at: https://doi.org/10.5281/zenodo.19493652
Large auxiliary datasets (including earthquake catalogs and gravity grids) required for full reproduction are available at: https://doi.org/10.5281/zenodo.19784141
All datasets correspond to the versions used in this study, ensuring full independent reproducibility of the analysis.

Acknowledgements. The author acknowledges the International Heat Flow Commission (IHFC) for maintaining the Global Heat Flow Database, and the researchers and institutions responsible for developing and making publicly available the GEM Global Active Faults Database, the PB2002 plate-boundary model, the UTIG/NOAA typed plate-boundary dataset, CRUST1.0, the global ocean-floor age grid, the Global Strain Rate Model, the World Gravity Map, and the earthquake catalogues used in this study.

Declaration of generative AI use. During preparation of the manuscript, the author used ChatGPT and Codex (OpenAI, GPT-5) as auxiliary tools for language editing, assisted translation, improvement of readability, document organization, and code documentation. These tools were not used to generate primary data, perform statistical analyses, or formulate the scientific interpretations. The author is responsible for the entire content of the manuscript.

Competing interests. The author declares no competing interests.

References

Bird, P. (2003). An updated digital model of plate boundaries, Geochem. Geophys. Geosyst., 4, 3, 1027, doi:10.1029/2001GC000252.

Bonvalot, S., G. Balmino, A. Briais, M. Kuhn et al. (2012). World Gravity Map, BGI-CGMW-CNES-IRD, Paris, doi:10.18168/bgi.23.

Courtillot, V., A. Davaille, J. Besse and J. Stock (2003). Three distinct types of hotspots in the Earth's mantle, Earth Planet. Sci. Lett., 205, 3-4, 295-308, doi:10.1016/S0012-821X(02)01048-8.

Davies, G. F. (1980). Review of oceanic and global heat flow estimates, Rev. Geophys. Space Phys., 18, 3, 718-722, doi:10.1029/RG018i003p00718.

Davies, J. H. (2013). Global map of solid Earth surface heat flow, Geochem. Geophys. Geosyst., 14, 10, 4608-4622, doi:10.1002/ggge.20271.

Davies, J. H. and D. R. Davies (2010). Earth's surface heat flux, Solid Earth, 1, 1, 5-24, doi:10.5194/se-1-5-2010.

Fuchs, S., B. Norden, F. Neumann, N. Kaul et al. (2023). Quality-assurance of heat-flow data: The new structure and evaluation scheme of the IHFC Global Heat Flow Database, Tectonophysics, 863, 229976, doi:10.1016/j.tecto.2023.229976.

Furlong, K. P. and D. S. Chapman (2013). Heat flow, heat generation, and the thermal state of the lithosphere, Annu. Rev. Earth Planet. Sci., 41, 385-410, doi:10.1146/annurev.earth.031208.100051.

Goutorbe, B., F. Lucazeau and A. Bonneville (2011). Global heat flow trends resolved from multiple geological and geophysical proxies, Geophys. J. Int., 187, 3, 1405-1419, doi:10.1111/j.1365-246X.2011.05228.x.

Hasterok, D. and D. S. Chapman (2011). Heat production and geotherms for the continental lithosphere, Earth Planet. Sci. Lett., 307, 1-2, 59-70, doi:10.1016/j.epsl.2011.04.034.

Jaupart, C., S. Labrosse, F. Lucazeau and J. C. Mareschal (2015). Temperatures, heat and energy in the mantle of the Earth, in G. Schubert (Editor), Treatise on Geophysics, Elsevier, 223-270, doi:10.1016/B978-0-444-53802-4.00126-3.

Kreemer, C., G. Blewitt and E. C. Klein (2014). A geodetic plate motion and Global Strain Rate Model, Geochem. Geophys. Geosyst., 15, 10, 3849-3889, doi:10.1002/2014GC005407.

Laske, G., G. Masters, Z. Ma and M. Pasyanos (2013). Update on CRUST1.0 – a 1-degree global model of Earth's crust, EGU General Assembly 2013, Geophys. Res. Abstr., 15, EGU2013-2658.

Lucazeau, F. (2019). Analysis and mapping of an updated terrestrial heat flow data set, Geochem. Geophys. Geosyst., 20, 8, 4001-4024, doi:10.1029/2019GC008389.

Müller, R. D., M. Sdrolias, C. Gaina and W. R. Roest (2008). Age, spreading rates, and spreading asymmetry of the world's ocean crust, Geochem. Geophys. Geosyst., 9, Q04006, doi:10.1029/2007GC001743.

NOAA National Centers for Environmental Information (NCEI) (n.d.). Plate Boundaries (from UTIG). Global plate-boundary layer categorized as convergent, divergent, and transform boundaries, https://gis.ngdc.noaa.gov/arcgis/rest/services/web_mercator/hazards/MapServer/12.

Pollack, H. N., S. J. Hurter and J. R. Johnson (1993). Heat flow from the Earth's interior: Analysis of the global data set, Rev. Geophys., 31, 3, 267-280, doi:10.1029/93RG01249.

Sclater, J. G. and J. Francheteau (1970). The implications of terrestrial heat flow observations on current tectonic and geochemical models of the crust and upper mantle of the Earth, Geophys. J. R. Astron. Soc., 20, 5, 509-542, doi:10.1111/j.1365-246X.1970.tb06089.x.

Sclater, J. G., C. Jaupart and D. A. Galson (1980). The heat flow through oceanic and continental crust and the heat loss of the Earth, Rev. Geophys., 18, 1, 269-311, doi:10.1029/RG018i001p00269.

Stål, T., A. M. Reading, S. Fuchs et al. (2022). Properties and biases of the global heat flow compilation, Front, Earth Sci., 10, 963525, doi:10.3389/feart.2022.963525.

Stein, C. A. and S. Stein (1992). A model for the global variation in oceanic depth and heat flow with lithospheric age, Nature, 359, 6391, 123-129, doi:10.1038/359123a0.

Styron, R. and M. Pagani (2020). The GEM Global Active Faults Database, Earthq. Spectra, 36, 1, 160-180, doi:10.1177/8755293020944182.

***CORRESPONDING AUTHOR: Cristiano GAUJAC**,
Independent researcher, Villefranche-sur-Saône, France
e-mail: papers.gaujac@gmail.com
© 2026 the Author(s).
Open Access. This article is licensed under a Creative Commons Attribution 4.0 International License